Journal of Materials Chemistry A

PAPER

View Article Online
View Journal | View Issue

Cite this: J. Mater. Chem. A, 2015, 3, 21343

Separating bulk from grain boundary Li ion conductivity in the sol–gel prepared solid electrolyte $Li_{1.5}Al_{0.5}Ti_{1.5}(PO_4)_3$

Stefan Breuer,*[a] Denise Prutsch,[a] Qianli Ma,[b] Viktor Epp,[a] Florian Preishuber-Pflügl,[a] Frank Tietz[bc] and Martin Wilkening*[a]

Lithium aluminium titanium phosphate (LATP) belongs to one of the most promising solid electrolytes. Besides sufficiently high electrochemical stability, its use in lithium-based all-solid-state batteries crucially depends on the ionic transport properties. While many impedance studies can be found in literature that report on overall ion conductivities, a discrimination of bulk and grain boundary electrical responses *via* conductivity spectroscopy has rarely been reported so far. Here, we took advantage of impedance measurements that were carried out at low temperatures to separate bulk contributions from the grain boundary responses. It turned out that bulk ion conductivity is by at least three orders of magnitude higher than ion transport across the grain boundary regions. At temperatures well below ambient long-range Li ion dynamics is governed by activation energies ranging from 0.26 to 0.29 eV depending on the sintering conditions. As an example, at temperatures as low as 173 K, the bulk ion conductivity, measured in N_2 inert gas atmosphere, is in the order of 8.1×10^{-6} S cm^{-1}. Extrapolating this value to room temperature yields *ca.* 3.4×10^{-3} S cm^{-1} at 293 K. Interestingly, exposing the dense pellets to air atmosphere over a long period of time causes a significant decrease of bulk ion transport. This process can be reversed if the phosphate is calcined at elevated temperatures again.

Received 14th August 2015
Accepted 19th September 2015

DOI: 10.1039/c5ta06379e

www.rsc.org/MaterialsA

1 Introduction

The interest in powerful electrochemical energy storage systems has tremendously increased over the last couple of years. In particular, the development of all-solid-state batteries taking advantage of solid electrolytes with high ion conductivity[1–9] represents one of the growing fields in energy science. Such systems would allow higher operation temperatures as well as the use of Li metal anodes directly increasing the energy density. Moreover, in contrast to systems using flammable liquid electrolytes, solid-state batteries should benefit from increased cycling stability and lifetime due to less ageing processes; as a consequence thereof, a significant increase in safety is expected.

A suitable solid electrolyte should guarantee electrochemical stability coupled with fast ion dynamics and negligible electronic conductivity. In recent years, garnet-type oxides[10–13] and argyrodite-type sulfides[14–16] entered the limelight; in addition, there is renewed interest in lithium aluminium titanium phosphates[17] $Li_{1+x}Al_xTi_{2-x}(PO_4)_3$ ($0 < x < 0.5$; LATP) crystallising with NASICON-type (Na superionic conductor) structure[18–23] that is based on $Na_{1+x}Zr_2Si_xP_{3-x}O_{12}$, $0 < x < 3$. LATP crystallises with rhombohedral structure (space group $R\bar{3}c$, see Fig. 1) and offers various Li sites, such as M1, M2 and M3. The site occupancy is controlled by the amount of substituted Al^{3+} cations which replace the Ti^{4+} ions.[17,21,24] The extra Li ions, which are needed for charge compensation, are anticipated to occupy the M3 sites.

Although a quite large number of studies[1,10] have been published that present new synthesis routes for oxides and deal with the characterisation of the overall ion transport properties by means of impedance spectroscopy, investigations focusing on the separation of the bulk and grain boundary electrical responses are less frequent.[25] To design, however, electrolytes with high ionic conductivity we need to know the key processes that govern both (i) bulk ion dynamics and (ii) ion transport across the grain boundaries or near the interfacial regions. Here, we took advantage of low-temperature impedance and conductivity spectroscopy to elucidate long-range ion dynamics inside the crystal lattice of LATP.[25] For this purpose a sol–gel prepared sample with the composition $Li_{1.5}Al_{0.5}Ti_{1.5}(PO_4)_3$ was used to perform impedance measurements from the mHz to the MHz range. In general, compared to solid-state preparation techniques the use of solution-based synthesis methods, as it is

[a]Christian Doppler Laboratory for Lithium Batteries and Institute for Chemistry and Technology of Materials, Graz University of Technology (NAWI Graz), Stremayrgasse 9, 8010 Graz, Austria
[b]Forschungszentrum Jülich GmbH, Institute of Energy and Climate Research, Materials Synthesis and Processing (IEK-1), 52425 Jülich, Germany
[c]Helmholtz Institute Münster, c/o Forschungszentrum Jülich GmbH, 52425 Jülich, Germany

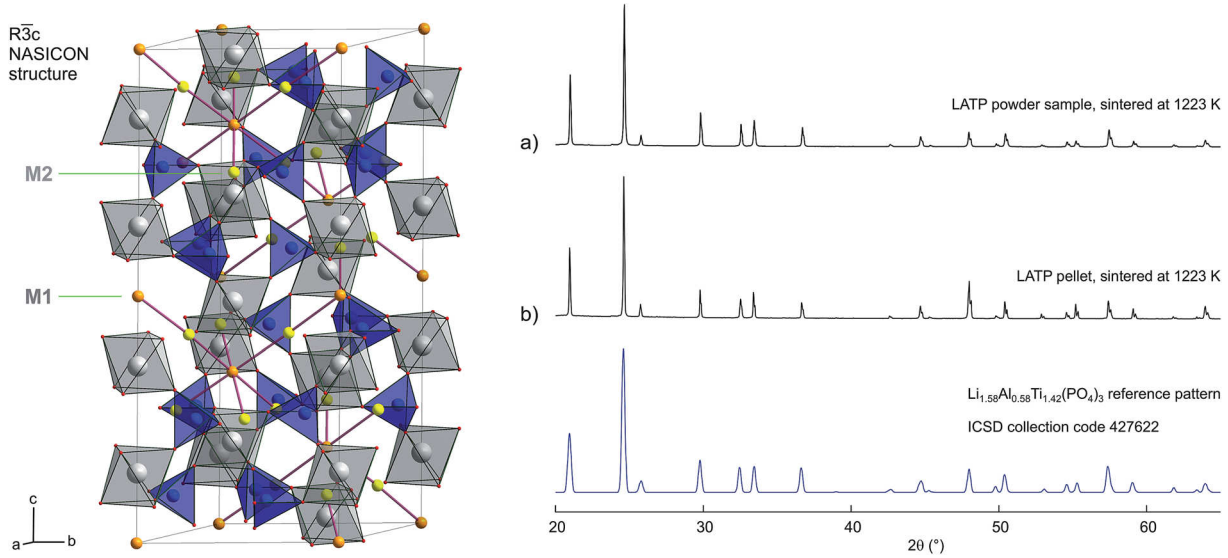

Fig. 1 Left: Crystal structure of LATP that is based on the NASICON type. As an example, orange and yellow spheres represent possible Li sites the ions may use to diffuse through the crystal lattice. Right: X-ray powder diffraction patterns of the powder sample investigated (a) and the pellet (b); both patterns were recorded after a sintering step at 1273 K. At the bottom a reference pattern (ICSD 427622) is given. The pattern were recorded after the conductivity measurements.

performed here, offers the possibility to better control composition, homogeneity and morphology of the final product.

Remarkably, it turned out that at a temperature of 173 K the ionic bulk conductivity of the sol–gel prepared phosphate $Li_{1.5}Al_{0.5}Ti_{1.5}(PO_4)_3$ is in the order of 8.1×10^{-6} S cm^{-1}. This translates, after extrapolation to room temperature, into a value of *ca.* 3.4×10^{-3} S cm^{-1} at 293 K, which is among the highest conductivities reported for LATP-based ion conductors.[17,20,26] It is even comparable with conductivities known for sulphides[4] such as $Li_{10}SnP_2S_{12}$ (4×10^{-3} S cm^{-1}) and the glass ceramic $Li_7P_3S_{11}$ (3.2×10^{-3} S cm^{-1}).[27,28] The corresponding activation energy E_a turns out to be approximately 0.26 eV. This value in between that of, *e.g.*, Al-stabilised garnet-based electrolytes (0.34 eV)[11] and argyrodite-type sulfides (0.20 eV).[16] Together with the fast ion conductor $Li_{10}GeP_2S_{12}$, which has been introduced by Kamaya *et al.*,[4] the latter belong to the best ion conductors presented over the last years.

2 Experimental

The $Li_{1.5}Al_{0.5}Ti_{1.5}(PO_4)_3$ sample was synthesized *via* a new sol–gel process. Stoichiometric amounts of $LiNO_3$ (99%, Alfa Aesar), $Al(NO_3)_3 \cdot 9H_2O$ (99%, Alfa Aesar), titanium(IV) isopropoxide (97%, Aldrich) and $NH_4H_2PO_4$ (99%, Merck) were used. At first, titanium(IV) isopropoxide (97%, Aldrich) was added into deionized water immediately forming a precipitate of titanium hydroxide. The fresh precipitate was filtered, washed and dissolved in nitric acid (65%, Aldrich). After a clear TiO^{2+} nitrate solution had been formed, a twofold molar amount of citric acid monohydrate (99%, Merck) was added into the solution to stabilise it. $LiNO_3$ and $Al(NO_3)_3 \cdot 9H_2O$ were then added into the TiO^{2+} nitrate solution while stirring. After the salts were dissolved, $NH_4H_2PO_4$ was added to the solution; this led to the formation of a sol. Stirring was maintained for another 0.5 h. After about 1 h, a stiff gel was spontaneously obtained. The gel was dried, calcined and milled in ethanol with zirconia balls on a milling bench. The ball-milled powder was put into a cylindrical pressing mold (10 mm in diameter, 4 mm in thickness) and pressed at a uniaxial pressure of 100 MPa. The pressed pellets were then sintered at 1123 K. Pure white samples with rhombohedral phase (Fig. 1) were obtained after sintering. The density of the pellets was over 95% of the theoretical density.

Immediately before the conductivity and impedance measurements, the pellet annealed at 1123 K was once again dried at 873 K for 16 hours to remove any moisture on its surface. Au electrodes of *ca.* 100 nm in thickness were applied using a sputter coater (Leica). The impedance measurements were carried out on a Novocontrol Concept 80 broadband dielectric spectrometer at frequencies ranging from 0.1 Hz to 10 MHz. The temperature was varied from 123 K to 423 K using either a stream of heated nitrogen gas or a constant flow of cold nitrogen in the cryostat. Any contamination with water or carbon dioxide was avoided as best as possible.

In order to use the same pellet for further impedance investigations, the Au layer was sanded down and the surface polished afterwards. Then, the specimen was annealed at 1223 K for 16 hours again; the density remained almost the same. Subsequently, impedances measurements were carried out under the same conditions in order to test the impact of sintering conditions on conductivity properties.

For comparison, also a powder sample of $Li_{1.5}Al_{0.5}Ti_{1.5}(PO_4)_3$ was investigated by impedance spectroscopy. A cylindrical pellet with a diameter of 5 mm and a thickness of *ca.* 1.2 mm was produced by pressing the pristine powder at a uniaxial pressure of approximately 0.5 GPa; the powder sample is a green body pellet with a density of reaching almost 90%. After

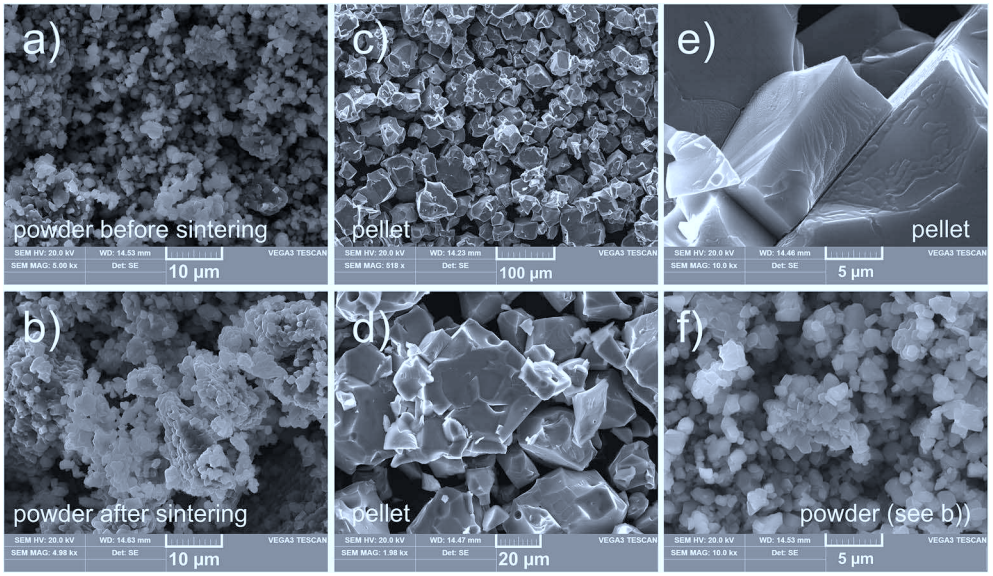

Fig. 2 SEM images of the powder sample ((a), (b) and (f)) as well as the pellet investigated ((c)–(e), just differing by the magnification). Except the one shown in (a) all images were taken after the sintering step at 1223 K and the conductivity measurements. (b) and (f) refer to the same sample; the images differ in magnification.

the drying process (873 K for 16 hours, see above), Li ion blocking electrodes with a thickness of *ca.* 100 nm were again applied at each side by Au sputtering. For comparison, the powder was also used to prepare a pellet that was sintered at 1223 K for 16 h.

The pellet as well as the samples prepared from the LATP powder were investigated by scanning electron microscopy (SEM) using a VEGA3 (Tescan) before and after the sintering steps (see Fig. 2). X-ray powder diffraction (D8 Advance, Bruker) using Cu-K_α radiation was employed to check the phase purity of the samples prepared.

3 Results and discussion

The phase purity of the samples investigated was examined by X-ray powder diffraction (XRD) carried out before and after the conductivity measurements. Apart from an 'order–disorder' transition, LATP shows no phase transformation down to 100 K.[29] The samples investigated in the present study reveal the diffraction pattern expected for $Li_{1.5}Al_{0.5}Ti_{1.5}(PO_4)_3$. In Fig. 1 (right) the pattern of $Li_{1.58}Al_{0.58}Ti_{1.42}(PO_4)_3$ (ICSD 427662) crystallising with the NASICON structure serves as a reference to check the purity of the samples with respect to additional crystalline phases. Since no other than the reflections of LATP were observed, such impurity phases are absent within the detection limit of X-ray diffraction. Because a flat background signal is seen with no humps that indicates amorphous material, we deal with highly crystalline samples. The narrow reflections of the XRD powder pattern indicate crystallites with diameters in the µm range. This observation is corroborated by our SEM investigations (see Fig. 2) revealing large crystallites in the case of the sintered pellet, in particular.

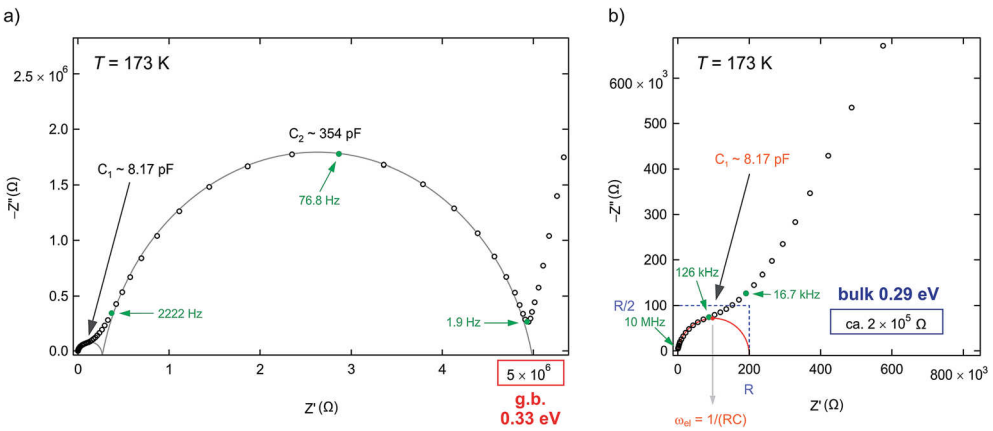

Fig. 3 (a) Complex plane plot, *i.e.*, AC-impedance diagram, of the $Li_{1.5}Al_{0.5}Ti_{1.5}(PO_4)_3$ pellet sintered at 1123 K. In (b) a magnification of the high-frequency region is shown. The highest frequency used to measure the data was 10 MHz. The solid line shows a fit using individual resistances and CPEs connected in parallel; see text for further discussion.

In Fig. 3(a) and (b) a typical complex plane plot, *i.e.*, the imaginary part $-Z''$ of the impedance is shown *vs.* its real part, Z', is displayed for the $Li_{1.5}Al_{0.5}Ti_{1.5}(PO_4)_3$ pellet, which was sintered at 1123 K. By using a relatively thick sample, 4 mm in the present case, the Nyquist plot is definitely composed of two semi-circles that can be satisfactorily separated on the frequency scale if the data are recorded at temperatures as low as 173 K. In Fig. 3(b) the high-frequency region of the plot is enlarged. The solid line in (a) and (b) represents a fit (ZView software) using an equivalent circuit that consists of a resistor R and a constant phase element CPE connected in parallel for each circle: $(R_1CPE_1)(R_2CPE_2)$. The resulting capacities are $C_1 = 8.2$ pF and $C_2 = 354$ pF for the arc at high and low frequencies, respectively (see Fig. 3). They are in agreement with those that can be directly derived *via* the maximum condition $\omega_{el} = 1/(RC)$, see Fig. 2(b), where the relaxation frequency is given by $\omega_{el} = 2\pi\nu$. A value of 8.2 pF clearly points to bulk ion dynamics, whereas a value larger than 300 pF can be attributed to the grain boundary (g.b.) response.[30]

The spike seen at the lowest frequencies represents electrode polarisation that needs not to be taken into account in the analysis of the impedance curve. At temperatures higher than ambient, only the g.b. arc and the near-vertical line associated to electrode polarisation is visible.

Interestingly, the two resistances R_1 and R_2 differ by more than one order of magnitude. Thus, Li motion across the grain boundaries in our LATP sample is significantly reduced as compared to intragranular ion hopping. At 173 K the bulk resistance R_1 is in the order of 200 kΩ while R_2 is in the MΩ range. Such differences between ion transport in the grain interior and overall conductivity were also reported by Arbi *et al.* earlier.[31] This suggests that manipulation of the microstructure could be used to improve the total conductivity, *e.g.*, by increasing the grain size and minimizing the number of grain boundaries. As has been shown for highly conducting sulphides, see, *e.g.*, the study of Hayashi on Na_3PS_4,[32] in the case of a glass ceramic pellet, the g.b. regions are largely reduced and seem to have a much less blocking effect on overall ion transport. Quite recently, Ma *et al.* used transmission electron microscopy to visualize the structural and chemical characteristics of ion blocking g.b. in $(Li_{3x}La_{2/3-x})TiO_3$.[33]

The features of (i) electrode polarisation, (ii) electrical bulk response and (iii) g.b. response also appear in the corresponding conductivity spectra, which we used to analyse the data as a function of temperature. In Fig. 4 collections of conductivity spectra, that is, the real part, σ', of the complex conductivity plotted *vs.* frequency ν, is shown for the pellet sintered at 1123 K (a) and 1223 K (b). Whereas at elevated temperatures both the g.b. response and electrode polarisation govern the spectra, at lower T the bulk response comes to light. Considerable polarisation effects are seen because of sufficiently fast Li ion transport causing a piling up of ions in front of the surface of the ion blocking electrode applied. While the low-frequency g.b. response yields distinct and almost flat DC plateaus, characterised by σ_{P1} (see Fig. 4(a)), those of the bulk response, σ_{P2}, are more difficult to analyse. Fortunately, at sufficiently low temperatures, see, *e.g.*, the isotherms at 153 K and 173 K, it is possible to read off reliable conductivities representing long-range Li ion transport through the crystal lattice of LATP. This analysis was also performed for the pellet that was sintered at 1273 K, see Fig. 4(b), although the determination of the inflection point of the isotherms turns out to be even more difficult. It is worth noting that the inverse of the values of σ_{P1} and σ_{P2} agree well with those deduced from the Nyquist plots, *viz.* R_1 and R_2.

The characteristics of both bulk and g.b. responses are also visible when the imaginary part $-Z''$ of the complex impedance is plotted *vs.* frequency, see Fig. 5. While the maximum at low frequencies is assigned to ion dynamics governed by grain boundaries, the local maximum at higher frequencies represents lattice ion dynamics. Since the electric modulus M'' is inversely proportional to the capacitance C, in a $\log_{10}(M''(\nu))$ plot bulk contributions are pronounced while the responses

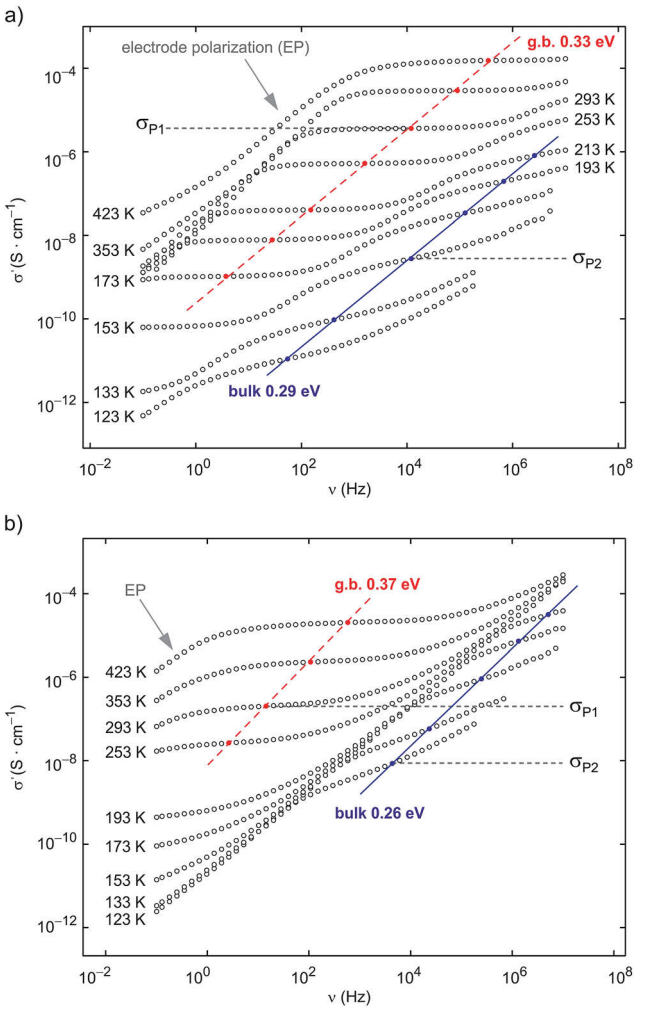

Fig. 4 (a) Conductivity isotherms of a sintered LATP pellet ($Li_{1.5}Al_{0.5}Ti_{1.5}(PO_4)_3$) with a thickness of 4 mm. The pellet was sintered at 1123 K. In (b) the corresponding isotherms of the same sample are shown after sintering at 1223 K. The conductivity spectra exhibit two separate plateaus reflecting grain boundary (g.b.) and bulk ion conductivities: σ_{P1} and σ_{P2}. EP denotes electrode polarisation because of the ion blocking electrodes used to record the data.

due to grain boundaries decrease in intensity.[30] The ratio of $C_2/C_1 = 43$ (see above) agrees well with $1/(M''_{max,1}/M''_{max,2})$. As expected, increasing the temperature from 153 K to 173 K shifts the maxima in M'' and $-Z''$ towards higher frequencies.

To analyse the underlying temperature dependence of the electrical relaxation processes we evaluated the conductivity isotherms shown in Fig. 4. Plotting the DC conductivities inferred from the isotherms as a function of the inverse temperature in an Arrhenius diagram, the activation energy of the bulk response can be obtained (see Fig. 6). Starting with 0.29 eV for the pellet sintered at 1123 K, E_a slightly decreases to 0.26 eV after the same sample was sintered again at 1223 K. Simultaneously, the value for the g.b. response increases from 0.33 eV to 0.37 eV.

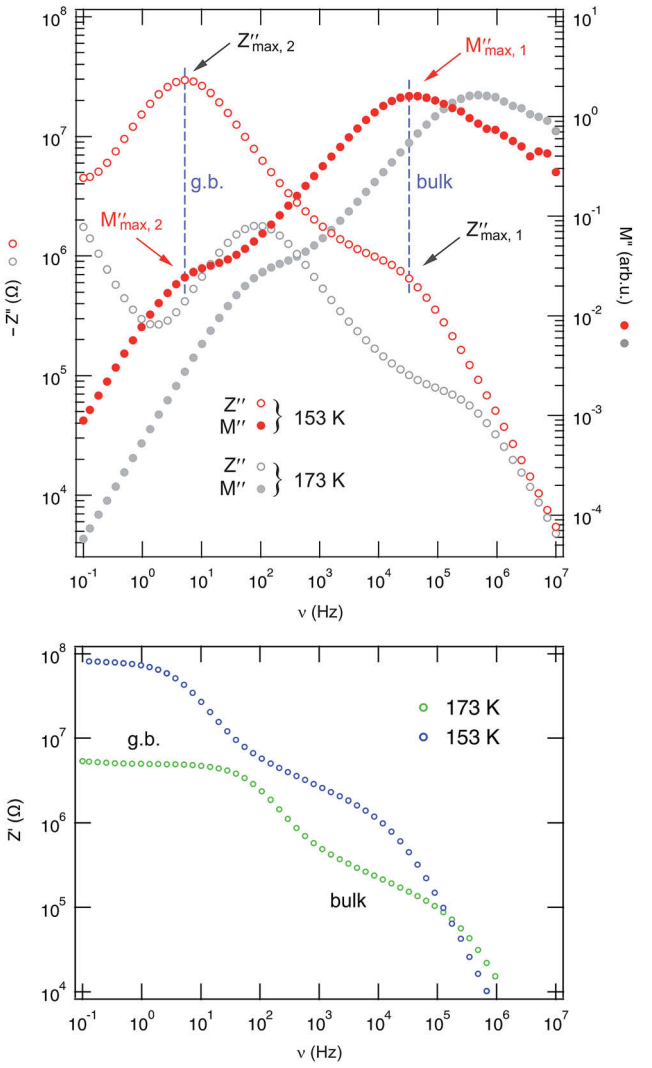

Fig. 5 Top: Change of the imaginary part of the complex impedance of $Li_{1.5}Al_{0.5}Ti_{1.5}(PO_4)_3$ with frequency. The curves exhibit two maxima that are ascribed to bulk and g.b. response. The maximum associated with lattice ion dynamics is more pronounced in the modulus representation, see right axis. Besides the data recorded at 153 K, the two spectra acquired at 173 K are also shown. Bottom: Variation of the real part of the complex impedance with frequency. As in the case of $\sigma'(\nu)$ the bulk regions appear at higher frequencies.

If we extrapolate the bulk data towards higher temperatures, the bulk ion conductivity would be in the order of 3.4 mS cm^{-1} at room temperature (see Fig. 6). This value, exceeding that reported by Fu for a glass ceramic (1.3 mS cm^{-1}),[26] is in good agreement with the results reported by several groups studying LATP-based solid electrolytes (see Table 1). In particular, it agrees well with the data measured by Arbi *et al.* quite recently.[31,34] This makes crystalline LATP indeed an extremely fast ion conductor with superior conductivity properties. Its exact bulk ion conductivity, however, depends on the sintering conditions chosen and can be somewhat tuned by post-annealing. The origins of this conductivity increase are, however, still unknown. Since the activation energy does not depend much on the sintering conditions, one might suppose a small change in the number of charge carriers that are allowed to move over long distances. Further work is needed to clarify the microstructural changes and alterations of the defect chemistry taking place during the high-T sintering steps. Of course, Li loss might change local Li^+ environments as well as Li and Al site occupancies in LATP.

Interestingly, if the pellet sample is exposed to ambient air for several days, a decrease of the bulk ion conductivity is observed by about two orders of magnitude, see the dashed-dotted line in Fig. 6. The feature is completely reversible: drying the sample at 873 K for 16 h resets the initially found high conductivity values. We attribute this effect to the influence of moisture on ion dynamics; further studies are in progress to elucidate the change in conductivity. Irrespective of the conductivity drop observed here, recent studies have been published that demonstrate the usability of water-stable LATP as electrolyte in aqueous battery systems such as Li–air batteries.[35] Moreover, LATP turned out to be relatively resistant to static corrosion in a hot, aqueous LiOH solution.[36]

Comparing our activation energies with those recently presented in literature, there is good agreement with recent studies.[34,37] Values slightly below 0.3 eV seem to accurately describe bulk long-range ion transport. Considering the work by Bucharsky *et al.*,[38] the authors found the same influence of sintering on ionic conductivity. Their activation energies are, however, higher than our values and range from 0.42 eV to 0.37 eV depending on the sintering temperature (850 °C to 1100 °C). Worth noting, we have re-calculated the activation energies using the data of Bucharsky *et al.*[38] because there is an error in their publication, which leads to much smaller values for E_a: the authors calculated activation energies from a $\log_{10}$ plot but forgot to take into account the conversion factor of $\log(e) \approx 2.3$ originating from the $\log_{10}$ to $\ln = \log_e$ (*logarithmus naturalis*) transformation. Hence, the activation energies announced by Bucharsky *et al.*[38] are by a factor of 0.43 too small. Although their absolute ion conductivities are quite high, *viz.* in the mS cm^{-1} range at ambient temperature, the activation energies resemble those we found for the grain boundary response.

For comparison, hopping barriers of *ca.* $E_a = 0.16$ eV were reported by Kosova *et al.*[48] Worth noting, such small activation energies were extracted from preliminary NMR relaxometry instead of conductivity spectroscopy. In contrast to conductivity measurements, NMR spin-lattice relaxation (SLR), when

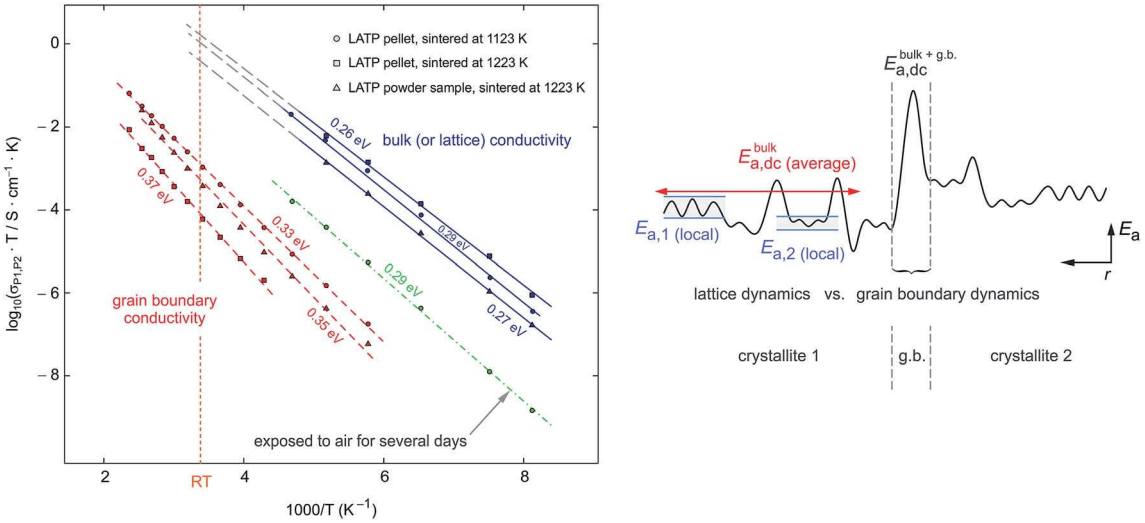

Fig. 6 Left: Arrhenius plot of the g.b. and bulk ion conductivities of the $Li_{1.5}Al_{0.5}Ti_{1.5}(PO_4)_3$ samples studied. The data were deduced from the conductivity isotherms partly shown in Fig. 3(a) and (b). The dashed and solid lines represent fits according to an Arrhenius law: $\sigma T \propto \exp(-E_a/(k_B T))$, k_B denotes Boltzmann's constant. The activation energies obtained are indicated. At ambient temperature, see vertical line, a DC bulk conductivity of *ca.* 3.4 mS cm^{-1} is obtained after extrapolation. Right: Schematic illustration of a heterogeneous potential landscape. Depending on the length scale, the method chosen to study ion dynamics is either sensitive to long-range ion dynamics or to local ionic jump processes. While atomic-scale methods, such as Li NMR, are also sensitive to individual ion hopping with low energy barriers, dc conductivity measurements probe an average value that characterises long-range, *i.e.*, through-going, ion dynamics.

Table 1 Overview of recent impedance measurements presented for LATP-based inorganic compounds in the literature

Composition $Li_{1+x}Al_xTi_{2-x}(PO_4)_3$	Synthesis method, reference	Conductivity (300 K)	Activation energy	Notes
$x = 0$, 0.2, 0.4	Solid state reaction, Arbi *et al.*[34]	3.4×10^{-3} S cm^{-1} (bulk)	0.24–0.28 eV ($x = 0.2$, 0.4)	Up to 3 GHz, 100–500 K
$x = 0.45$	Mechanochemical synthesis, Morimoto *et al.*[39]	2.9×10^{-4} S cm^{-1}	0.31 eV	Annealing of amorphous powder
$x = 0.3$	Mechanochemical synthesis, Morimoto *et al.*[40]	*ca.* 10^{-4} S cm^{-1}	0.36 eV	Sintered at 1173 K
$x = 0.3$	Citrate sol–gel process, Kunshina *et al.*[41]	3–4 $\times 10^{-4}$ S cm^{-1}	0.21 eV	Sintered at 1273 K, 293–473 K, up to 1 MHz; 86–90% density
$x = 0.3$	Wet chemical synthesis, Duluard *et al.*[42]	1.6×10^{-4} S cm^{-1}	—	Densified, 97%
$x = 0.3$	Samples obtained from Ceramatec Inc., Jackman *et al.*[43]	6.7×10^{-4} S cm^{-1}	0.31–0.36 eV	Effect of micro-cracking
$x = 0.3$	Citric acid-assisted sol–gel process, Yoon *et al.*[44]	7.8×10^{-5} S cm^{-1} (g.b.) 9.4×10^{-4} S cm^{-1} (bulk)	0.395 eV (total); 0.13 eV (bulk)	
Composition unknown, glass ceramic	Samples obtained from Ohara Inc., Mariappan *et al.*[45]	10^{-5} to 10^{-6} S cm^{-1} (190 K)	0.37 eV (total); 0.33 eV (bulk)	Total and bulk conductivity differ by one order of magnitude; 0.1–10 MHz
$x = 0.5$	Co-precipitation method, Kotobuki *et al.*[46]	1.4×10^{-3} S cm^{-1} (bulk) 1.5×10^{-4} S cm^{-1} (total)	0.31 eV	Sintered at 1323 K
$x = 0.5$	Co-precipitation method, Kotobuki *et al.*[47]	1.2–3.1 $\times 10^{-3}$ S cm^{-1} (bulk) 7.1×10^{-7} to 4.5×10^{-4} S cm^{-1} (total)	0.13–0.19 eV (bulk) 0.28–0.35 eV (total)	Bulk and overall conductivity depends on the Al source used: $Al(NO_3)_3$, $Al(C_3H_7O)_3$
$x = 0.5$	Crystallisation of a glass, Narváez-Semanate and Rodrigues[37]	1.3×10^{-3} S cm^{-1}	0.27 eV	Glass ceramic, several samples, sintered at 973 K to 1273 K, see also references therein

performed in the laboratory frame of reference, in particular, is sensitive to both long-range and local Li jump processes depending on the conditions used to collect the data. While values in the order of 0.3 eV refer to through-going (that is, long-range) ion transport in the bulk, activation energies from SLR NMR, on the other hand, have to be carefully analysed. In many cases they reflect the elementary steps of ion jumping, *i.e.*, diffusion processes on a shorter length scale than usually accessible by conductivity spectroscopy or AC impedance measurements, respectively.

Our own NMR relaxometry measurements, which were carried out in both the rotating and laboratory frame of reference point to very similar activation energies ranging from 0.16 to 0.18 eV only.[49] Most importantly, the barriers seen *via* NMR have to be attributed to two different diffusion processes the ions are subject to almost simultaneously. At higher temperatures NMR was able to sense a third diffusion process with a higher energy barrier. Thus, NMR activation energies as low as 0.16 eV indeed characterise individual hopping processes rather than the averaged, long-range ion transport seen *via* Li ion conductivity measurements. Quite recently, Lang *et al.*[50] studied Li ion hopping using first-principle methods based on density functional theory. The authors report an interstitial diffusion mechanism that is characterised by an activation energy of 0.19 eV.[50]

4 Conclusions

$Li_{1+x}Al_xTi_{2-x}(PO_4)_3$ belongs to the group of solid electrolytes which are expected to largely influence the development of all-solid-state batteries. A sufficiently high ion conductivity, being in the same order of magnitude as that of a liquid electrolyte, is one of the basic requirements needed. So far, the separate study of bulk and grain boundary conductivity has only rarely been documented. Here, we took advantage of low temperature conductivity measurements and impedance spectroscopy to study bulk ion dynamics at temperatures lower than 215 K. In this temperature range Li ion transport through the lattice is governed by an average activation $E_{a,\sigma}$ of only 0.26 eV when a pellet sample is considered that was annealed at 950 °C. The grain boundary response is determined by notably larger activation energies ranging from 0.33 eV to 0.37 eV; the exact value depends on the sintering temperature applied.

We could further show that even bulk ionic conductivity seems to depend on the sintering conditions. Exposing the samples to ambient air for a long period of time slows down ion transport. The effect is reversible: after annealing the same pellet at elevated temperature, the original high ion conductivity is observed again. We attribute this finding to the influence of moisture on Li ion dynamics.

When compared with results from NMR spectroscopy and DFT calculations presented in the literature so far, we have to keep in mind that DC conductivity measurements probe long-range ion transport while NMR is sensitive to the local barriers between next neighbouring Li ions. Moreover, whereas $E_{a,\sigma}$ represents an average over the whole potential landscape, Li NMR is able to characterise individual diffusion processes whose superposition results in overall ion transport measured by conductivity spectroscopy in the so-called low-frequency range, *i.e.*, the DC limit.

Acknowledgements

We thank our colleagues at the TU Graz for valuable discussions. Financial support by the Deutsche Forschungsgemeinschaft (DFG Research Unit 1277, grant no. WI3600/2-2 and 4-1) as well as by the Austrian Federal Ministry of Science, Research and Economy, and the Austrian National Foundation for Research, Technology and Development (CD-Laboratory of Lithium Batteries: Ageing Effects, Technology and New Materials) is greatly appreciated.

References

1 J. Sakamoto, in *Handbook of Solid State Batteries*, World Scientific, 2015, pp. 391–414.
2 K. Takada, *Acta Mater.*, 2013, **61**, 759–770.
3 P. Knauth, *Solid State Ionics*, 2009, **180**, 911–916.
4 N. Kamaya, K. Homma, Y. Yamakawa, M. Hirayama, R. Kanno, M. Yonemura, T. Kamiyama, Y. Kato, S. Hama, K. Kawamoto and A. Mitsui, *Nat. Mater.*, 2011, **10**, 682–686.
5 A. Hayashi and M. Tatsumisago, *Electron. Mater. Lett.*, 2012, **8**, 199–207.
6 M. Tatsumisago and A. Hayashi, *Int. J. Appl. Glass Sci.*, 2014, **5**, 226–235.
7 V. Epp and M. Wilkening, in *Handbook of Solid State Batteries*, World Scientific, 2015, pp. 133–190.
8 K. Minami, F. Mizuno, A. Hayashi and M. Tatsumisago, *Solid State Ionics*, 2007, **178**, 837–841.
9 M. Park, X. Zhang, M. Chung, G. B. Less and A. M. Sastry, *J. Power Sources*, 2010, **195**, 7904–7929.
10 V. Thangadurai, S. Narayanan and D. Pinzaru, *Chem. Soc. Rev.*, 2014, **43**, 4714–4727.
11 H. Buschmann, J. Dölle, S. Berendts, A. Kuhn, P. Bottke, M. Wilkening, P. Heitjans, A. Senyshyn, H. Ehrenberg, A. Lotnyk, V. Duppel, L. Kienle and J. Janek, *Phys. Chem. Chem. Phys.*, 2011, **13**, 19378–19392.
12 A. Kuhn, S. Narayanan, L. Spencer, G. Goward, V. Thangadurai and M. Wilkening, *Phys. Rev. B: Condens. Matter Mater. Phys.*, 2011, **83**, 094302.
13 S. Narayanan, V. Epp, M. Wilkening and V. Thangadurai, *RSC Adv.*, 2012, **2**, 2553–2561.
14 H. Deiseroth, S. Kong, H. Eckert, J. Vannahme, C. Reiner, T. Zaiß and M. Schlosser, *Angew. Chem.*, 2008, **120**, 767–770.
15 O. Pecher, S. T. Kong, T. Goebel, V. Nickel, K. Weichert, C. Reiner, H. J. Deiseroth, J. Maier, F. Haarmann and D. Zahn, *Chem.–Eur. J.*, 2010, **16**, 8349–8354.
16 V. Epp, Ö. Gün, H.-J. Deiseroth and M. Wilkening, *J. Phys. Chem. Lett.*, 2013, **4**, 2118–2123.
17 H. Aono, E. Sugimoto, Y. Sadaoka, N. Imanaka and G. Adachi, *J. Electrochem. Soc.*, 1990, **137**, 1023–1027.
18 H. Aono, E. Sugimoto, Y. Sadaoka, N. Imanaka and G. Adachi, *J. Electrochem. Soc.*, 1989, **136**, 590–591.
19 J. Fu, *J. Am. Ceram. Soc.*, 1997, **80**, 1901–1903.

20 K. Takahashi, J. Ohmura, D. Im, D. J. Lee, T. Zhang, N. Imanishi, A. Hirano, M. B. Phillipps, Y. Takeda and O. Yamamoto, *J. Electrochem. Soc.*, 2012, **159**, A342–A348.
21 P. Maldonado-Manso, E. R. Losilla, M. Martínez-Lara, M. A. G. Aranda, S. Bruque, F. E. Mouahid and M. Zahir, *Chem. Mater.*, 2003, **15**, 1879–1885.
22 F. E. Mouahid, M. Zahir, P. Maldonado-Manso, S. Bruque, E. R. Losilla, D. Chimie, C. Doukkali and E. Jadida, *J. Mater. Chem.*, 2001, **3**, 3258–3263.
23 K. Takada, M. Tansho, I. Yanase, T. Inada, A. Kajiyama, M. Kouguchi, S. Kondo and M. Watanabe, *Solid State Ionics*, 2001, **139**, 241–247.
24 J. Fu, *J. Mater. Sci.*, 1998, **33**, 1549–1553.
25 W. E. Tenhaeff, E. Rangasamy, Y. Wang, A. P. Sokolov, J. Wolfenstine, J. Sakamoto and N. J. Dudney, *ChemElectroChem*, 2014, **1**, 375–378.
26 J. Fu, *Solid State Ionics*, 1997, **96**, 195–200.
27 P. Bron, S. Johansson, K. Zick, J. Schmedt auf der Günne, S. Dehnen and B. Roling, *J. Am. Chem. Soc.*, 2013, **135**, 15694–15697.
28 F. Mizuno, A. Hayashi, K. Tadanaga and M. Tatsumisago, *Adv. Mater.*, 2005, **17**, 918–921.
29 I. Y. Pinus, A. V. Khoroshilov, K. S. Gavrichev, V. P. Tarasov and A. B. Yaroslavtsev, *Solid State Ionics*, 2012, **212**, 112–116.
30 J. T. S. Irvine, D. C. Sinclair and A. R. West, *Adv. Mater.*, 1990, **2**, 132–138.
31 K. Arbi, S. Mandal, J. M. Rojo and J. Sanz, *Chem. Mater.*, 2002, **14**, 1091–1097.
32 A. Hayashi, K. Noi, A. Sakuda and M. Tatsumisago, *Nat. Commun.*, 2012, **3**, 856–860.
33 C. Ma, K. Chen, C. Liang, C.-W. Nan, R. Ishikawa, K. More and M. Chi, *Energy Environ. Sci.*, 2014, **7**, 1638–1642.
34 K. Arbi, W. Bucheli, R. Jiménez and J. Sanz, *J. Eur. Ceram. Soc.*, 2015, **35**, 1477–1484.
35 S. Hasegawa, N. Imanishi, T. Zhang, J. Xie, A. Hirano, Y. Takeda and O. Yamamoto, *J. Power Sources*, 2009, **189**, 371–377.
36 S. D. Jackman and R. A. Cutler, *J. Power Sources*, 2013, **230**, 251–260.
37 J. L. Narváez-Semanate and A. C. M. Rodrigues, *Solid State Ionics*, 2010, **181**, 1197–1204.
38 E. C. Bucharsky, K. G. Schell, A. Hintennach and M. J. Hoffmann, *Solid State Ionics*, 2015, **274**, 77–82.
39 H. Morimoto, M. Hirukawa, A. Matsumoto, T. Kurahayashi, N. Ito and S. Tobishima, *Electrochemistry*, 2014, **82**, 870–874.
40 H. Morimoto, H. Awano, J. Terashima, Y. Shindo, S. Nakanishi, N. Ito, K. Ishikawa and S. I. Tobishima, *J. Power Sources*, 2013, **240**, 636–643.
41 G. B. Kunshina, O. G. Gromov, E. P. Lokshin and V. T. Kalinnikov, *Russ. J. Inorg. Chem.*, 2014, **59**, 424–430.
42 S. Duluard, A. Paillassa, L. Puech, P. Vinatier, V. Turq, P. Rozier, P. Lenormand, P. L. Taberna, P. Simon and F. Ansart, *J. Eur. Ceram. Soc.*, 2013, **33**, 1145–1153.
43 S. D. Jackman and R. A. Cutler, *J. Power Sources*, 2012, **218**, 65–72.
44 Y. Yoon, J. Kim, C. Park and D. Shin, *J. Ceram. Process. Res.*, 2013, **14**, 563–566.
45 C. R. Mariappan, *Appl. Phys. A: Mater. Sci. Process.*, 2014, **117**, 847–852.
46 M. Kotobuki, M. Koishi and Y. Kato, *Ionics*, 2013, **19**, 1945–1948.
47 M. Kotobuki and M. Koishi, *Ceram. Int.*, 2012, **39**, 4645–4649.
48 N. V. Kosova, E. T. Devyatkina, A. P. Stepanov and A. L. Buzlukov, *Ionics*, 2008, **14**, 303–311.
49 V. Epp, Q. Ma, E.-M. Hammer, F. Tietz and M. Wilkening, 2015, unpublished results.
50 B. Lang, B. Ziebarth and C. Elsässer, *Chem. Mater.*, 2015, **27**, 5040–5048.

